Geoderma 429 (2023) 116267

Contents lists available at ScienceDirect

Geoderma

journal homepage: www.elsevier.com/locate/geoderma

Combining UAV remote sensing and pedological analyses to better understand soil piping erosion

Narges Kariminejad [a], Adel Sepehr [a,b,*], Jean Poesen [c,d], Ali Hassanli [e]

[a] Department of Desert and Arid Zones Management, Ferdowsi University of Mashhad (FUM), Mashhad, Iran
[b] Research Group of Environmental Hazards and Ecosystem Management, Ferdowsi University of Mashhad (FUM), Mashhad, Iran
[c] Department of Earth and Environmental Sciences, KU Leuven, Heverlee, Belgium
[d] Institute of Earth and Environmental Sciences, Maria Curie-Skłodowska University, Lublin, Poland
[e] Adjunct Professor at the University of South Australia, Mawson Lakes Campus, Australia

ARTICLE INFO

Handling Editor: Morgan Cristine L.S.

Keywords:
Piping system
Ground-penetrating radar
Electrical resistivity tomography
Soil horizons

ABSTRACT

The study and mapping of evidences of soil piping using non-destructive techniques is a key issue in quantitative geomorphology. This paper attempts to combine Aerial mapping systems (Unmanned Aerial Vehicles (UAV)), soil physical and chemical attributes, and near-surface geophysical survey tools (ground penetrating radar and electrical resistivity tomography) to provide a comprehensive understanding of geometric features of soil piping in arid and semi-arid regions. The UAV Mapping System was applied to prepare ortho-photos, topography, analytical hill shading, drainage density, and land use maps of two different piping sites (site 1: rangelands, and site 2: agricultural lands) in Sarakhs plain, Razavi Khorasan Province, northeastern Iran. The physical and chemical soil attributes were analyzed in six soil profiles to check the hypothesis that these soil attributes control the occurrence of piping-related features (i.e., sinkhole, blind gully, gully), and to test if there are any differences in soil properties between the two land use types. The near surface geophysical tools were used to determine the approximate size of soil pipes, and to simulate their internal structure. The results of the derived UAV's independent variables confirmed that typical soil erosion features related to piping (i.e., sinkhole, blind gully, gully) developed exactly in adjustment with subsurface processes (i.e., drainage density). The quantitative algorithms of pedology revealed significant differences of Na^+ and SAR for soil profiles with and without piping erosion, but these soil properties themselves are not enough to explain piping development at the two study sites. The volume of GPR line surveys was 1701.5 m^3 in site 1 and 1203 m^3 in site 2. The potential distribution of subsurface pipes revealed by applying GPR were more extensive than those deduced from soil surface observations: three-dimensional pipe number density (number of soil pipes per unit soil volume; # m^{-3}) of potential pipes and collapsed cavities simulated with a mean pipe length and pipe depth of 143.4 cm and 88 cm in rangelands and 175.75 cm and 79.14 cm in agricultural lands, respectively. The maximum density of pipes or pipe roof collapses occurred within soil depth boundaries of 0–50 cm at site 1 and 30–100 cm at site 2. The ratio of surface erosion features to subsurface potential piping in rangeland and agricultural lands was ca. 26.1 % and 10.4 %, respectively. The electrical resistivity tomography (ERT) measurements indicated higher resistivity values in piping-prone areas, where pipes were initiated at the bedrock interface. Integrating all data obtained by different techniques in this study allowed to better understand the extent of piping erosion in both surface and subsurface soil horizons.

1. Introduction

A complicated system to quantify, piping erosion was less contemplated compared to flows over the land surface causing soil erosion (Boucher, 1990; Wilson et al., 2018). As a remarkable contributor of storm runoff, piping erosion occurs firstly in soil macropores and the result of this process is not visible at the surface until the pipe roof collapses (Verachtert et al., 2010; Wilson et al., 2012; Bernatek-Jakiel et al., 2016). Most researchers reported erosion processes producing small surface depressions caused by slow subsurface soil erosion or by

* Corresponding author at: Department of Desert and Arid Zones Management, Ferdowsi University of Mashhad (FUM), Mashhad, Iran.
E-mail address: adelsepehr@um.ac.ir (A. Sepehr).

https://doi.org/10.1016/j.geoderma.2022.116267
Received 21 April 2022; Received in revised form 12 October 2022; Accepted 10 November 2022
Available online 18 November 2022

dramatic and sudden sinkhole formation due to the soil surface collapse above larger cavities. The initiation and development of soil pipes occurs below the soil surface (Galarowski, 1976; Verachtert et al., 2013). Piping erosion in a natural landscape visibly expands in different regions across the world (Poesen, 2018). Natural piping is recognized as a hydrological and geomorphological process in many environments (Bryan and Jones, 1997; Chappell and Sherlock, 2005; Verachtert et al., 2010). Due to the presence of piping phenomena in many regions around the globe, these erosive landforms resulting in the erosion of the subsoil, significant soil losses and the creation of subsurface flow lines. These intensify the subsurface runoff discharge and the formation of drainage lines enhancing sediment transport (Bernatek-Jakiel and Poesen, 2018). Natural pipes functioning as belowground drainage networks transfer large volumes of water, sediments and nutrients (Holden et al., 2002; Jones, 2010; Smart et al., 2013) and extend as self-a propagating process (Wilson et al., 2015) resulting in a change of the hydrological response of hillslopes (Wilson et al., 2018).

Meanwhile, piping erosion considered as a more episodic process rather than a periodic or seasonal one (Starkel, 2006) was involved with channel extension through soil roof collapse often forming gullies (Poesen et al., 1996). Piping systems as a compound of connected pipes lead at the soil surface to soil collapses, sinkholes, dendritic patterns of erosion channels (rills), and gully erosion in regions with erodible soils. They are closely associated with gully head migration processes and gully sidewall failure (Verachtert et al., 2010; Zhu, 2012; Bernatek-Jakiel and Poesen, 2018). Several researchers report characteristics of soil piping and its related processes (Bryan and Jones, 1997; Wilson et al., 2012) in a wide range of regions such as loess-mantled and mountainous areas, badlands, and peatlands (e.g., Poesen et al. 1996; Faulkner, 2006; Bernatek-Jakiel et al., 2016). The field mapping of piping networks was also detected by dye tracing, smoke bombs, soil coring (e.g., Botschek et al., 2002; Bíl and Kubeček, 2012; Wilson et al., 2015). A better understanding of these processes needs to consider different properties of the belowground soil structure (Jones, 2004; Kariminejad et al., 2021). Because soil pipes cannot easily be examined and interpreted through simple observations at the soil surface (Jones, 2004; Robinson et al., 2013; Kariminejad et al., 2021), more efforts are required to apply techniques for studying the spatial patterns, dimensions and activity of subsurface pipes. Utilizing appropriate techniques is also needed to monitor internal soil erosion and to detect the evolution of soil pipes in erodible soils.

Developing measurement techniques to detect piping erosion taking network densities into account, represents a key geomorphological challenge (Holden et al., 2002; Cappadonia et al., 2015; Got et al., 2014). Recently, detection of soil pipe networks was done by applying UAVs as a non-destructive tool in erodible soils (Hamshaw, et al., 2019; Mayr, et al., 2019; Hosseinalizadeh et al., 2019). These studies underline the importance of quantitative techniques to detect and map pipes and pipe networks. In this regard, geophysical techniques (GPR, ground penetrating radar and ERT, electrical resistivity tomography) applied in geomorphological studies were evaluated by several researchers (Schrott and Sass; 2008; Sjödahl et al., 2009; Migoń et al., 2014; Podgorski et al., 2015; Kasprzak et al., 2017; Bovi et al., 2020). The GPR particularly detects cavities or collapse sinkholes (Van Schoor, 2002; Carbonel et al., 2014; Bernatek-Jakiel and Kondracka, 2016) and has been used to investigate the earth materials in dams exposed to piping failure (Panthulu et al., 2001; Oh and Sun, 2008). The ERT has been used to monitor seepage (Johansson and Dahlin, 1996), to determine differences in electrical properties of water-soil mixtures (Panthulu et al., 2001; Oh, 2012), and to delineate weak spots in the core materials of earthen dams (Panthulu et al., 2001; Oh, and Sun; 2008). Integrating two data sets, researchers achieved three-dimensional images with GPR and ERT of the potential spatial distribution of subsurface and surface erosion by soil piping (Reynolds, 2011; Bernatek-Jakiel et al., 2016; Evangelista et al., 2017; Bovi et al., 2020; Patti et al., 2021). These two non-invasive and cost-effective geophysical tools have the potential to detect soil pipes and to provide details of the subsurface soil, which are needed for natural piping hazard mitigation policy and planning of piping control measures.

Beside few reports, the use of geophysics in the detection of soil pipes processes is not yet widely investigated and little is known about the density of soil pipes (Holden et al., 2002; Got et al., 2014; Bernatek-Jakiel and Kondracka, 2016). As far as the authors are aware, very few studies have reported on vertical soil properties and their relation to potential pipe formation in the subsoil or collapsed cavities (Bovi et al., 2020; Bernatek-Jakiel and Kondracka, 2022). This study attempts to fill a scientific gap through improved understanding and better detection of potential soil pipes in two semi-arid areas under two land use types (i.e., rangelands and agricultural lands). The main objectives were: (1) to detect the internal pathway of collapsed pipes based on the UAV-drivers (i.e., drainage density), (2) to assess the soil properties which may be associated with the interpretation of geophysical data affecting soil pipe development, (3) to estimate the geometric properties (i.e., depth, volume, density) of potential soil pipes based on subsurface and surface investigations, (4) to reconstruct the internal structure of soil materials associated with soil piping, and (5) to define the differences between piping-associated soil erosion features (i.e., sinkholes, blind gullies, gullies) in rangelands and agricultural lands by combining near surface geophysics and hydrogeomorphology.

2. Study area

Two regions were selected based on the occurrence of piping processes and sinkhole forms. Both study areas are located in Sarakhs, Khorasan Razavi province, Iran. Fig. 1 shows the location and topographic characteristics of the two study sites in Sarakhs catchment.

The first study site (site 1 in Fig. 1), Takhte-Soltan (35° 5́9 N and 60° 2́0 E) was given the status of a protected area for Asian cheetahs. The land use at this site is rangeland. It is a single hillslope covering an area of 55.91 ha and having a minimum and maximum elevation of 542 and 579 m a.s.l., respectively. The dominant soil texture is clay loam. It is a hilly region with a semi-arid climate (steppe), based on the Koppen climate classification. The mean annual rainfall depth is 202 mm, and the mean annual air temperature is 27 °C. The second study site (site 2 in Fig. 1), Shorluq (36° 1́9 N and 6́0 38° E) is near one of the villages of the Marzdaran section of Sarakhs city and covers an area of 79.34 ha. Shorluq is located at 54 km southwest of Sarakhs city, at the border of the Sarakhs- Kashfrud River. The minimum and maximum elevation of the second site are 815 and 865 m a.s.l., respectively and it has a temperate and dry mountainous climate. The dominant soil texture in this region is clay. The seasonal Shurluq river flows near this site, which is connected to the Kashfrud River. The land use at the second site is agricultural land. The main occupation of people living in this village is agriculture and animal husbandry. The main crops produced are wheat and barley. Geomorphologically, site 1 has been classified as a bare pediment (younger alluvial plain), though site 2 is located in a covered pediment (an aggregation area with sediments and deposits). The younger alluvial plain has the general dendritic drainage pattern which naturally leads to the development of soil erosional features (i.e., closed depression, dendritic erosion) in protected rangelands (site 1). However, the initiation of erosional landforms (i.e., sinkhole, blind gully) in the covered pediment is due to the accumulation of dissolved minerals through the hardpan mainly caused by land-use changes (agricultural land use).

3. Materials and methods

To prepare a comprehensive detection of the soil piping activity in the Sarakhs catchment, several techniques were applied: i.e., digital geomorphological mapping (UAV), determination of physical and chemical soil properties, and two geophysical techniques (ERT and GPR). We focused on the integration of several data types to cross-check

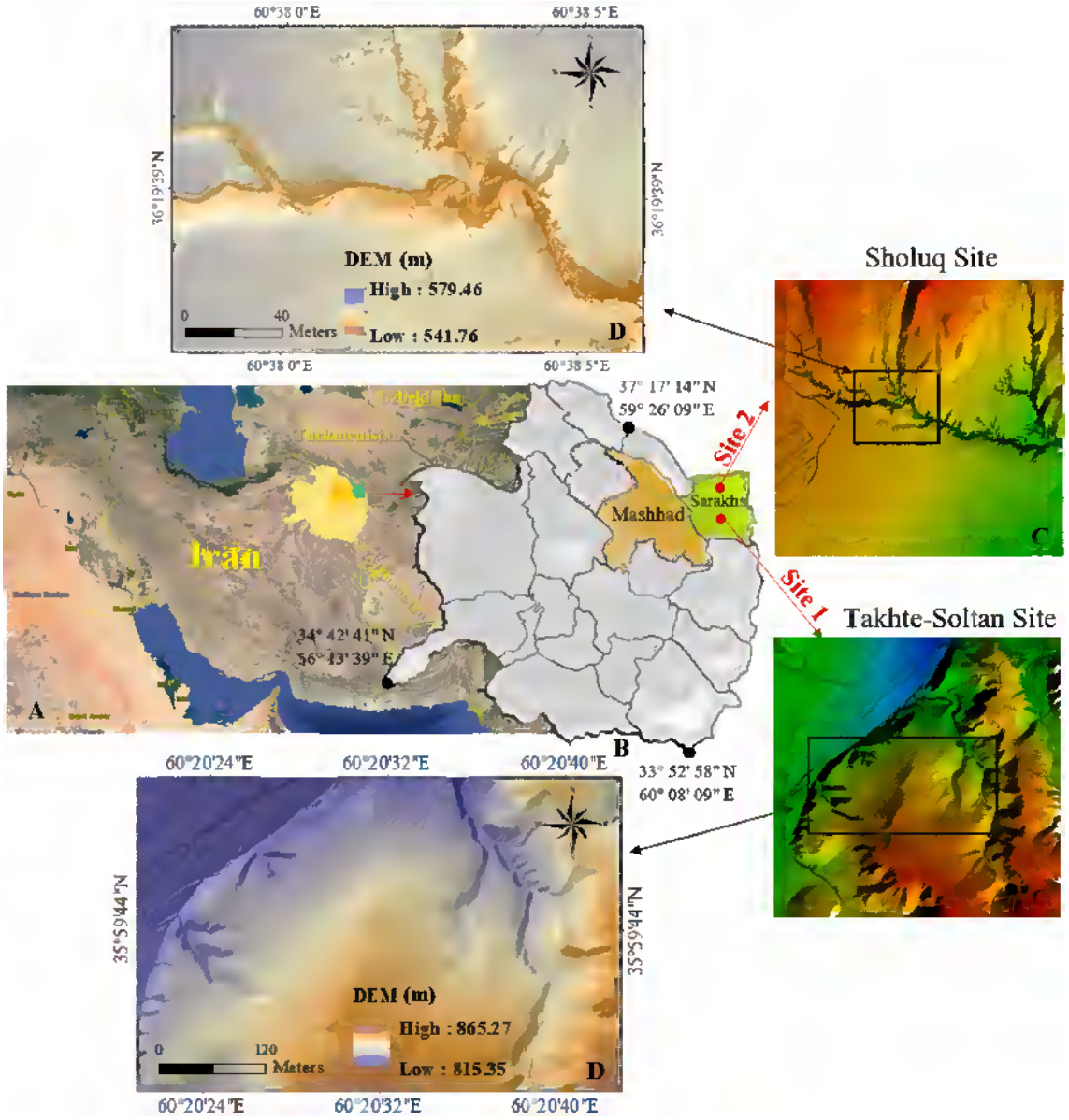

Fig. 1. (A) Sarakhs plain in Iran, (B) location of the two study sites, (C) orthophoto (aerial photograph) taken from the two selected sites (site 1 = Takhte-Soltan, site 2 = Shorluq), and digital elevation model (DEM, altitude in m) with spatial resolution of 0.15 × 0.15 cm obtained from unmanned aerial vehicle (D).

the subsurface pipe mechanisms and to decrease interpretation ambiguities. Fig. 2 illustrates the erosional landforms observed at the two study sites. The geomorphological mapping was done in two study regions, and the geophysical survey was obtained using 15 GPR profiles at site-1 and 13 GPR profiles at site-2 (4 ERT profiles for both sites). We measured physical and chemical soil properties from different horizons at six soil profiles to identify the main factors affecting erosional landforms. Fig. 3 shows the flowchart of the data collection methods made at the two study areas: i.e. geo-hydrological mapping, physical and chemical soil attributes, and geophysical tools.

3.1. Geo-hydrological mapping of soil piping

We applied unmanned aerial vehicles with a camera model FC6310_8.8_5472x3648 (RGB) and sensor dimensions of 12.833 (mm) * 8.556 (mm) at the two study sites. At site 1, average Ground Sampling Distance (GSD) was 2.70 cm in an area of 55.91 ha. The georeferencing was made for 6 Ground Control Points (mean RMS error = 0.01 m). The mean Reprojection Error (pixels) was 0.137. The digital surface model and orthomosaic resolution obtained was 2.7 cm/pixel. The number of calibrated images and geolocated images was 431 out of 431.

At site 2, the average GSD was 3.73 cm and the area covered 79.34 ha. The georeferencing was considered for 7 Ground Control Points (mean RMSerror = 0.019 m). The mean Reprojection Error (pixels) was 0.15. The DSM and orthomosaic resolution obtained was 3.73 cm/pixel. The number of calibrated Images and geolocated Images was 361 out of 361. The morphological characteristics (i.e., length, density, depth) of different soil erosional features and their magnitude was calculated by integration of UAV remote sensing data and field observations. The maps of dendritic landforms and drainage networks were also produced from the *ortho*-photo and DEM of UAV images.

3.2. Soil description and sampling strategy

Soil samples were collected from six representative soil profiles (three for each site with three sample replicates for each horizon) in different hillslope positions. At site 1, three soil profiles were selected based on the presence of rill erosion, closed depression, and a site

Fig. 2. Illustration of the erosional landforms at the two study sites (site 1 = Takhte-Soltan, site 2 = Shorluq). Site 1: A = Dendritic rill channel pattern with the main channel having a width of 0.6 m and mean depth of 0.75 m, B = gully heads consisting of a complex of surface and subsurface channels (pipes) and collapsed pipes in clay loam soil texture, and C = pipe outlets in a soil wall. Site 2: A and B = sinkholes formed by pipe roof collapse, and C = larger gully initiated by piping erosion.

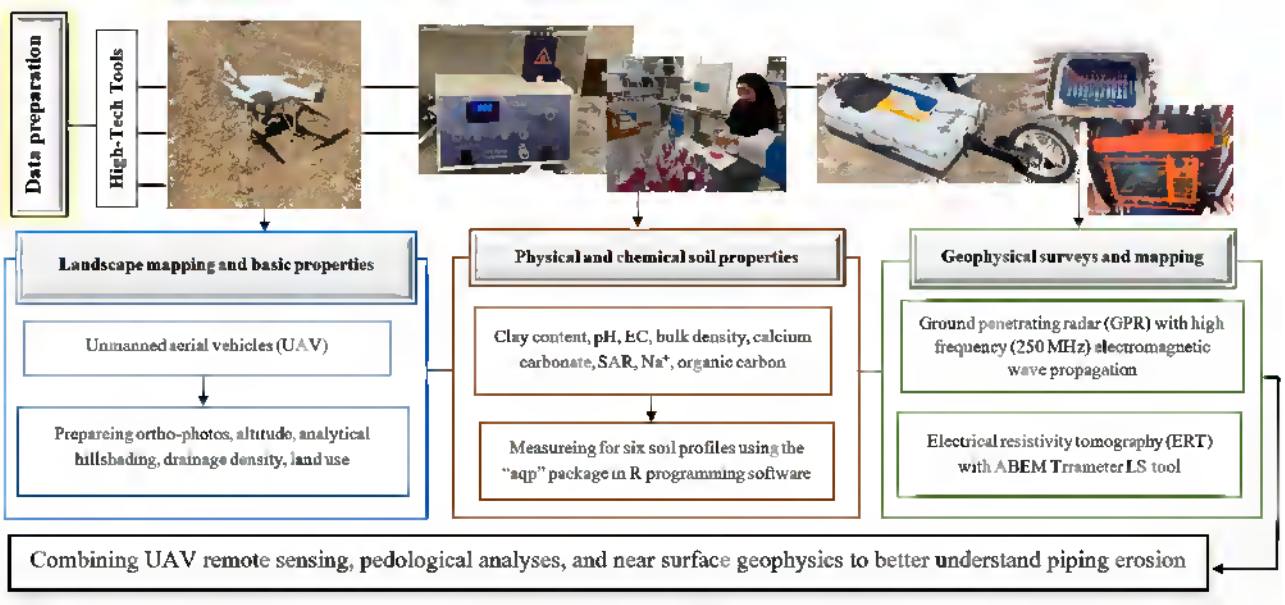

Fig. 3. Flowchart of data collection methods, showing the three main groups: aerial mapping systems, measurements of physical and chemical soil attributes, and geophysical surveys.

without erosional landforms. At site 2, three soil profiles were selected based on the location of a gully head, a sinkhole, and a site without erosional features (Fig. 4). The soil texture was classified using USDA classification. We measured all soil properties in the laboratory. The physical and chemical soil attributes (bulk density, soil texture, organic carbon, EC, pH, $CaCo_3$, Na^+, SAR) were analyzed in the laboratory and then processed using the "aqp" package in R programming software.

In the laboratory, all soil samples were air-dried and afterwards, fine earth (<2 mm) was separated (except for the preparation of bulk density samples) for further analysis. The Munsell scale is applied to define soil color on dry and moist soil samples. The soil texture was determined using the hydrometer method (Gee and Bauder, 1986). The total porosity and bulk density were estimated using the core method (Blake and Hartge, 1986). Soil pH was measured in a saturated sample dissolved with distilled water and 0.01 M $CaCl_2$ using a solution ratio of 1:1 for water and 1:2 ratio for $CaCl_2$. The organic carbon content was calculated based on rapid dichromate oxidation using modified Tyurin titrimetric method (Nelson and Sommers, 1983). The content of carbonate (CaCO3) was measured using the volumetric calcimeter technique (Loeppert and Suarez, 1996). The exchangeable cations were extracted by 1 M NH_4OAc buffered at pH 7. Electrical conductivity (dS/m) was measured by the Jenway 4510 conductivity meter. The Sodium Adsorption Ratio (SAR) was obtained using the following equation (Vasu et al., 2016):

$$SAR = \frac{Na^+}{\sqrt{\frac{Ca^{2+}+Mg^{2+}}{2}}}$$

The same procedure was applied to determine chemical and physical properties from all soil samples taken from each horizon (Fig. 5A, B). After measurement of the soil physical and chemical properties, the point data were stored in Microsoft excel spreadsheets, and the "aqp" package was applied as a main algorithm. This package was used to classify and visualize soil attributes in soil-profile collections within an open-source framework. The extended version of the "aqp" package (used in this study) was designed by R-Forge (http://aqp.r-forge.r-project.org). The functions of this package were successfully used to visually check the hypothesis that soil attributes control the presence of particular piping-related soil erosion features, and to test if there is any difference in soil properties between the two land use types.

3.3. Geophysics survey

Two geophysical methods have been applied to define piping-related features namely electrical resistivity tomography – ERT, and ground penetrating radar – GPR (Fig. 5C–F). In total, 28 georadar profiles and 4 ERT profiles of different lengths were made and used for further analyses. It is the combined use of these methods that allow to interpret the data presented in the results. A map of transects and soil sampling

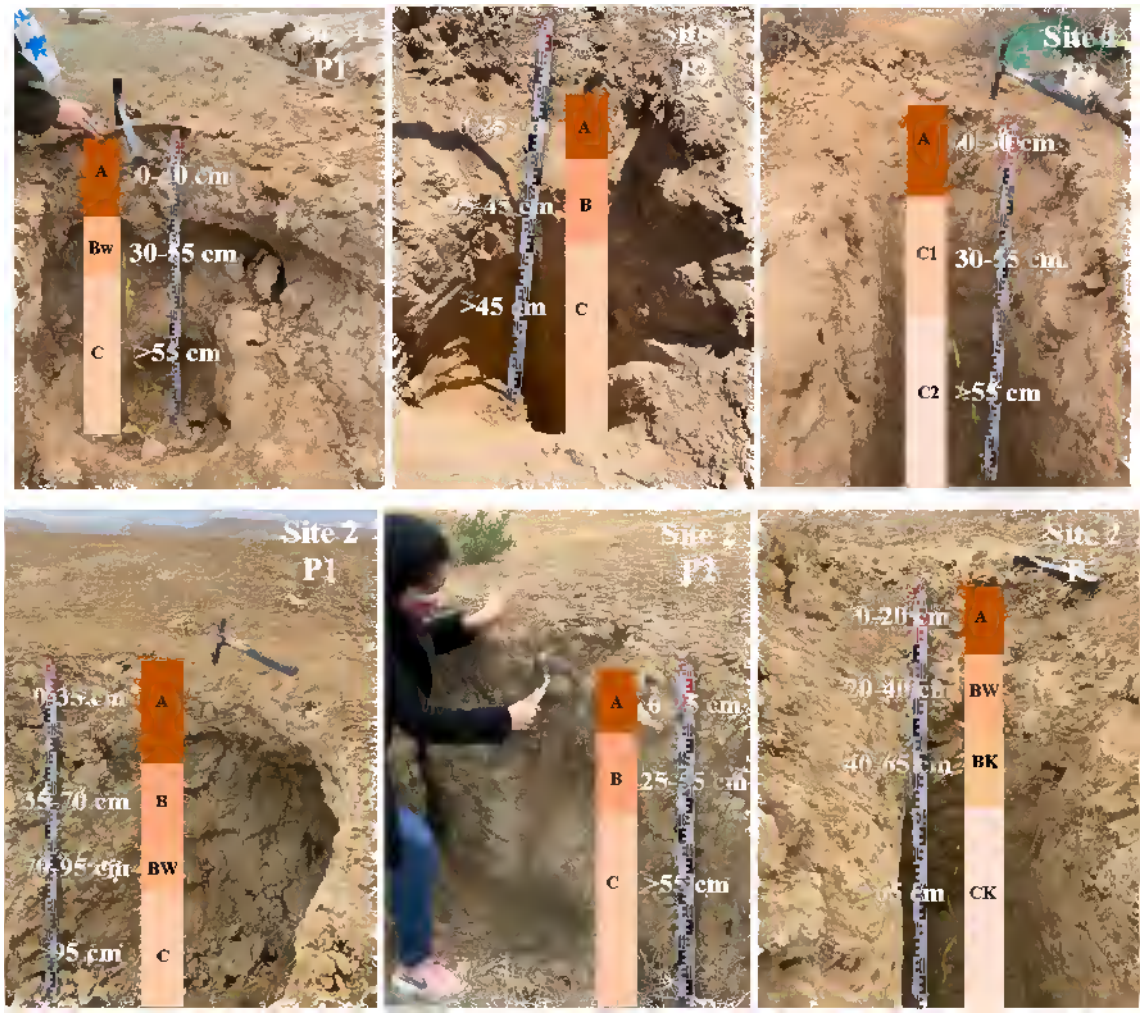

Fig. 4. Soil sampling from each soil horizon at locations with and without erosional landforms in site 1 (Takhte-Soltan) and site 2 (Shorluq). In site 1, three soil profiles were selected from the location with rill erosion (*P*1), closed depression (*P*2), and the location without such landforms (*P*3). In site 2, three soil profiles were selected from the location with a gully head (*P*1), a sinkhole (*P*2), and the location without erosional landforms (*P*3).

Fig. 5. Illustration of the laboratory and field measurements made at the two study sites. A = chemical analysis of soil samples, B = soil textural analysis, C = GPR at site 2, D = ERT at site 2, E = GPR at site 1, and F = ERT at site 1.

locations is shown in Fig. 6.

3.3.1. Ground penetrating radar

Of all non-destructive tools applied in soil pipe detection in various natural landscapes, GPR is the most quantitatively measurable geophysical technique, particularly to define the subsurface materials associated with changes in geological structure or changes in soil attributes, which may have a considerable impact on pipe development (Carbonel et al., 2014; Bernatek-Jakiel and Kondracka, 2016; Tandon et al., 2021). GPR is used to locate surface erosion features and subsurface features or lateral connectivity at the contact zone between the soil and the rock at shallow depths. In this method, very high frequency radio waves (10–3000 MHz) are sent into the soil where the waves are reflected by objects or a relatively clear boundary between the subsurface layers and then recorded in the form of mapping. The GPR method was performed using a transmitter antenna with an average frequency of 250 MHz and an X3M processor. In this process, background removal filters, gain adjustment, and other required filters are utilized. The velocity of electromagnetic waves inside the soil materials was about 0.08 m/ns. Since geophysical methods are based on the physical properties of soil materials and the identification factor is the difference between the physical parameters of materials and the environment, changes were considered accordingly and were interpreted as anomalies. So, the anomalies were related to the presence of cavities (soil pipes) and cracks up to a depth of 3 m. This means that these anomalies may be associated with biological activity, especially those located just below the surface (down to 50 cm soil depth). Probably some of these subsurface anomalies resulted from macropores made by burrowing animals creating preferential flow paths that favoured the transfer surface runoff from one tunnel to another and thus inducing subsurface flow erosion that transformed these tunnels. These tunnels might not always be detected because of the accuracy range of the antenna used in the study limits their detection. In this study, the GPR lines (horizontal and vertical in all directions) were randomly selected in the region with and without soil piping (P lines in site 1 and site 2) to obtain detailed information about the density of subsurface pipes or pipe roof collapses in the whole sampled area. The length of the GPR lines varied from 10 m to 90 m (overall 600 m in site 1 and 433 m in site 2). The soil pipes or pipe roof collapses were detected in the 0–3 m soil depth with the GPR and field observation. The volume of GPR line surveys was 1701.5 m^3 in site 1 and 1203 m^3 in site 2. The maximum width and depth of GPR lines were 2 m and 3 m, approximately. Following Verachtert et al. (2011), the volumes of the potential pipes and collapsed cavities were calculated assuming cylindrical pipe shapes ($V = \pi r^2 h$).

3.3.2. Electrical resistivity tomography

The ERT exploits the differences in electrical resistivity properties between soil, water, and it also detects cavities filled with air (Sjödahl et al., 2009). The ERT was obtained by an ABEM Terrameter LS IP&Rs acquisition system, in conjunction with a multi-electrode system, applying Wenner-Schlumberger configuration to acquire different investigation depth. Data acquisition was performed with an electrode spacing of 2.5 m for an array length of 55 m. The ERT was based on the flow of a constant current in the soil (direct or alternating current). In this study, 110 data points were selected in each ERT profile, and the value of electrical resistivity was detected in each point. After collecting the field data and reviewing and deleting or correcting the erroneous data, the inversion of the field data was performed using Res2Dinv software and the final cross-sections obtained for further analysis.

4. Results

In total, two orthophotos were taken from two sites covered by rangelands (site 1) and by agricultural land (site 2). In site 1 closed depressions, dendritic erosion features, as well as pipe outlets in gully walls were present. However, the bigger erosional landforms including sinkholes, discontinuous (blind) gullies, gully heads, and gullies were observed at site 2. The results regarding the morphological characteristics (i.e., length, density, depth) of these soil erosion features and their magnitude was calculated by integration of UAV remote sensing data

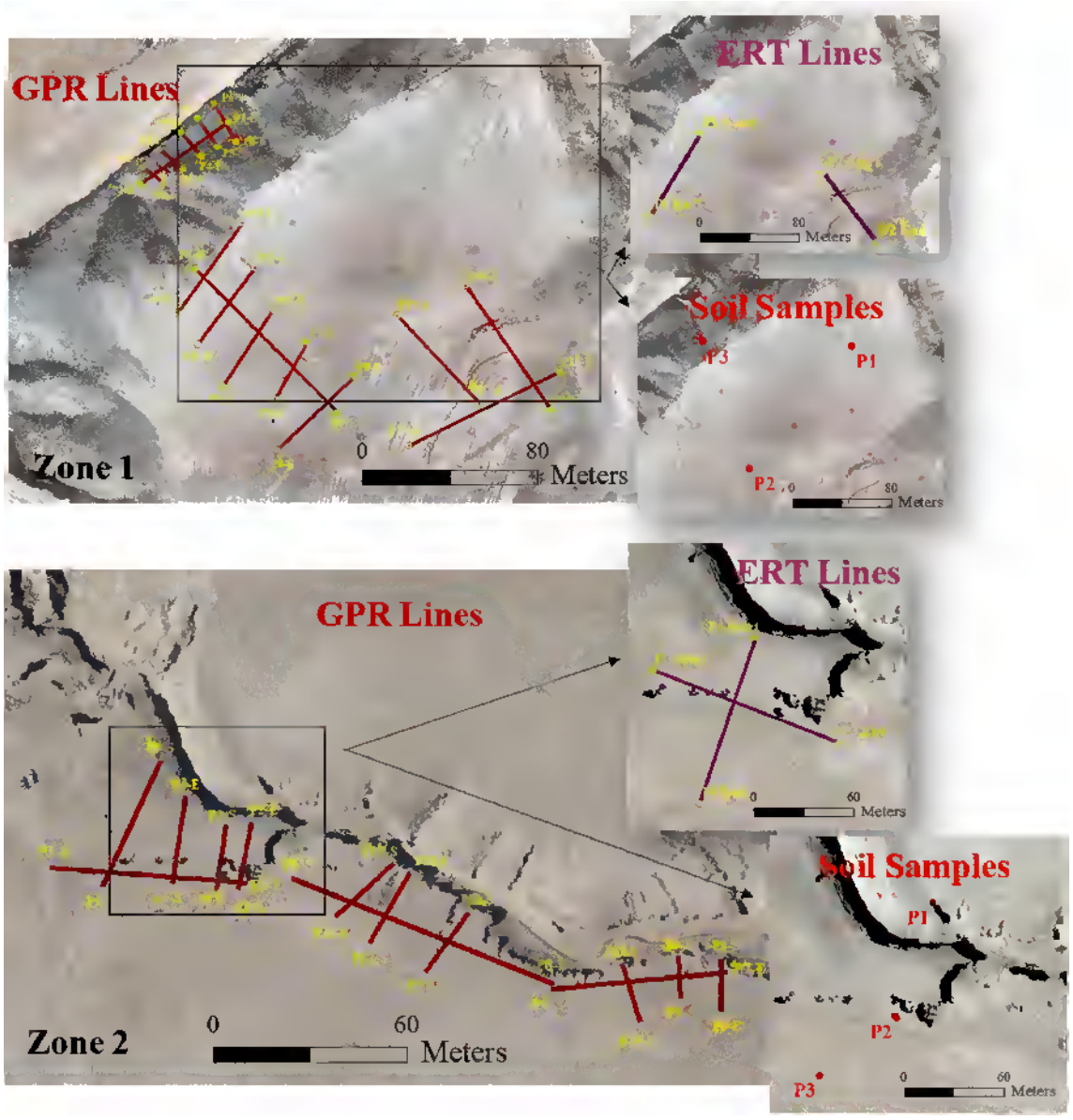

Fig. 6. Location of GPR and ERT transects (lines) as well as soil profiles placed over the *ortho*-photos at site 1 (Takhte-Soltan) and site 2 (Shorluq).

and field observations. In site 1, the closed depressions had an approximate mean width of 2.1 m and a mean length of 3. 2 m. The length of dendritic patterns of erosion channels (rills) in eroded rangelands was more than 15 m with a depth of approximately 1 m. This pattern coincided with the drainage network taken from the *ortho*-photo and DEM of UAV images (Fig. 7). In this figure the blue lines (channel networks) and their relation to mapped pipes and gullies showed how well these lines relate to these features. There was also a large gully with many pipe outlets at its wall. Pipes at outlets had a mean height of 0.4 m, a mean width of 0.5 m, and a density of 4 outlets per square meter of vertical gully wall. In site 2, the sinkholes were bigger and almost circular or oval in plan form, with a mean length of 3.4 m and a mean width of 2.2 m. The blind gullies were slightly wider (3.6 m) and longer (8.1 m) than the sinkholes. Pipe outlets had a mean height of 0.4 m, a mean width of 0.5 m, and a density of 1 outlet per square meter of vertical gully wall. The maximum depth of gullies exceeded 7 m. In this site, pipes developed at a depth of 0.9 m, similar to the mean depth of the mapped sinkholes.

The following soil properties were analyzed in the laboratory and then processed using R programming software: Na^{+}, clay content, organic carbon, EC, pH, $CaCO_3$, SAR, and bulk density. These soil attributes were visualized in six soil profiles using "aqp" package. The results for site 1 showed that areas with erosive landforms have considerable amounts of lime ($CaCO_3$) in the C horizon, where there is also a lot of silt. This site had fine and coarse pebbles at a soil depth of 30–60 cm. Although this site was a sedimentary basin and had a plain morphology, the whole region was not saline and alkaline. The Dry paint and Wet paint color were 10 YR (4/5) and 10 YR (4/4) based on Munsell Soil Color Charts (Color and (Firm), 2010). At site 2, erosional landforms, and particularly the gully heads generally had a cubic structure. The Dry paint and Wet paint color were 2.5 YR (3/5) and 2.5 YR (3/4) based on Munsell Soil Color Charts. Sinkholes have less lime ($CaCo_3$) in this site. In the regions without erosion, there was a high lime content in the B and C horizons. A simple diagram (Fig. 8) representing the horizon names and depths for a selection of soil profiles allows to describe the soils within the two studied regions. Based on Fig. 8A and E, the amount of sodium and SAR were the lowest at the two sites without erosion. The clay content in the A horizon at site 2 was higher than in the other horizons. The organic carbon content in both sites was <0.8 %, although the amount was higher in areas with erosion (i.e., closed depression, dendritic erosion features) in site 1. The percentage of CaCo3 in the soil

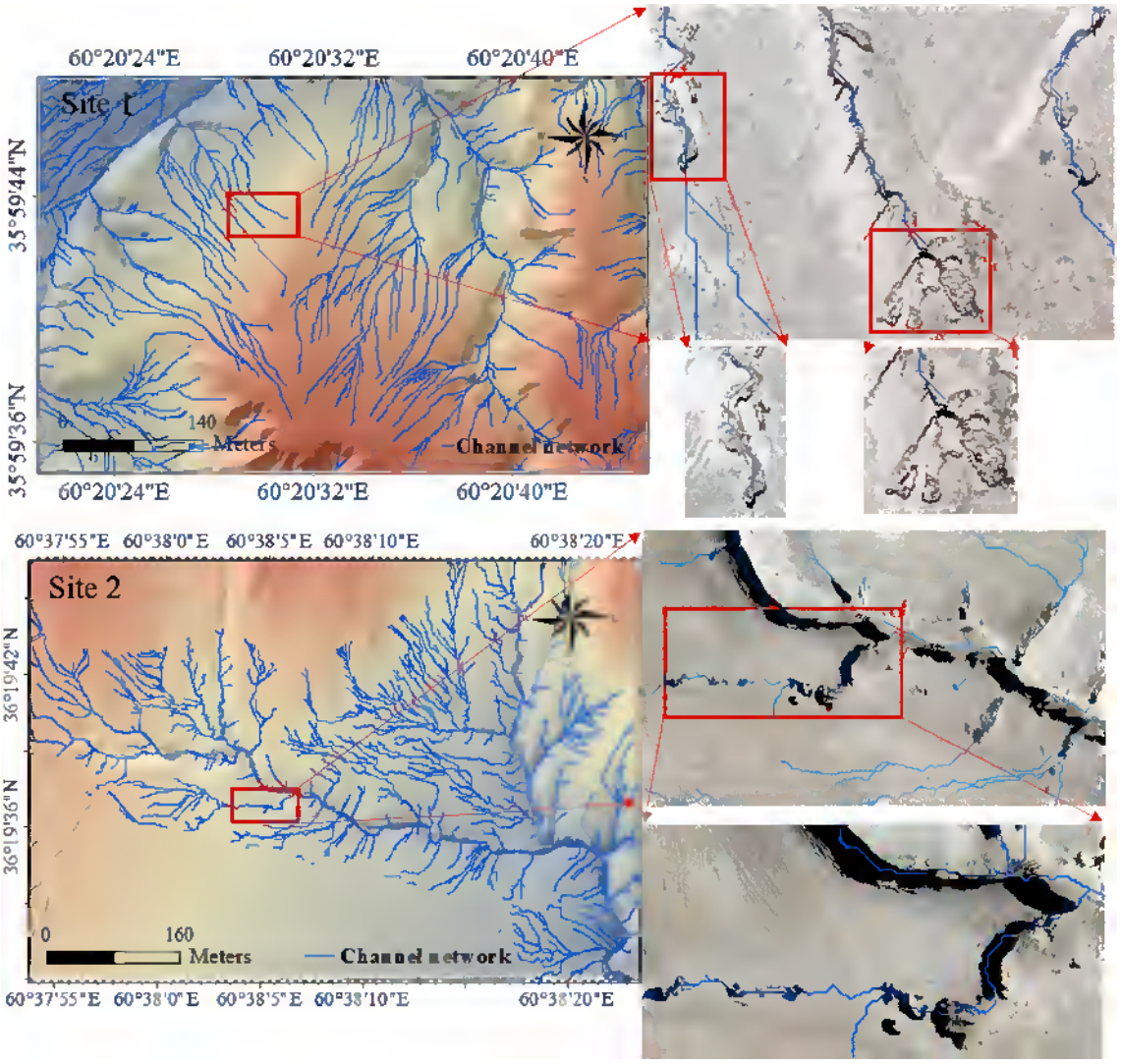

Fig. 7. The schematic maps of channel networks at site 1 (Takhte-Soltan) and at site 2 (Shorluq). The blue lines and their relation to mapped pipes and gullies show how well the lines correspond to the location of these features. The dendritic patterns of erosion channels (rills) or dendritic rill channel pattern can easily be recognized at site 1 with the largest channel having a width of 1.25 m and a mean depth of 0.85 m. (For interpretation of the references to color in this figure legend, the reader is referred to the web version of this article.)

horizons was not significantly different (except for the C horizon below the dendritic erosion features in the site 1 (68.75 %), and their average value in the site 1 was 13.86 % and in the site 2 was equal to 56.88 %. There was no significant difference in mean bulk density at the two sites with and without erosion. The average pH and EC in site 1 were 8.87 and 1.83 (dS/m), though they were 8.80 and 1.47 (dS/m) in site 2.

Regarding geophysical investigation using GPR (*P*1-P17 lines) shown in Fig. 6A, the mean pipe length at site 1 was approximately 143.4 cm, and the minimum and maximum values were about 40 cm and 400 cm. The average pipe depth was about 88 cm. This site was entirely located in rangeland. Three-dimensional pipe number density (number of soil pipes per unit soil volume; # m^{-3}) of potential pipes and collapsed cavities was 5.1 m^{-3}, and the volume density (volume of soil pipes per unit soil volume of GPR surveys over 3 m soil depth) was 0.2. The mean pipe volume was almost 2.8 m^3 for the whole surface and subsurface holes investigated by GPR lines (600 m) (Table 1). Fig. 9 illustrates some GPR profiles. The circles mark the places with a potential pipe or a collapsed cavity. As shown in Table 2, the volume of both surface erosion features and subsurface potential piping was approximately 293.5 m^3. The length and the volume of subsurface pipes were 161.3 m and 249.9 m^3. Accordingly, the volume fraction of surface erosion features to all soil pipes (i.e., both surface erosion features and subsurface potential piping) was about 0.15. Thus, the surface erosion features/subsurface potential piping ratio for pipe length and volume were almost 0.3 and 0.2 respectively. As already noted, these quantitative estimates of pipe size are associated with uncertainty due to the inherent vectoral nature of the GPR signals and the complex geological conditions of the subsurface soil materials (Jol, 2008).

At site 2, the GPR lines (*P*1-P13 shown in Fig. 6B) were measured, and then, the geometric features were calculated. The mean length of individual pipes was about 175.74 cm, and the minimum and maximum were 80 cm and 600 cm. The average pipe depth was 79.14 cm. Three-dimensional volumetric number density (# m^{-3}) (number of soil pipes per unit soil volume) of potential pipe and collapsed cavity was 1.76 m^{-3}, and the volume density of pipes (volume of pipes per unit soil volume of GPR surveys) was 0.21. The mean pipe volume was 2.88 m^3 for all the pipe holes calculated by GPR lines (433 m) (Table 1). As explained before, the GPR lines which were taken in both horizontal and vertical directions (Fig. 6B) were selected almost near to gullies where the surface landforms were spreading particularly in downstream of agricultural land. As shown in Table 2, the length and volume of surface pipes were 24.3 m and 23.6 m^3. The length and volume of subsurface

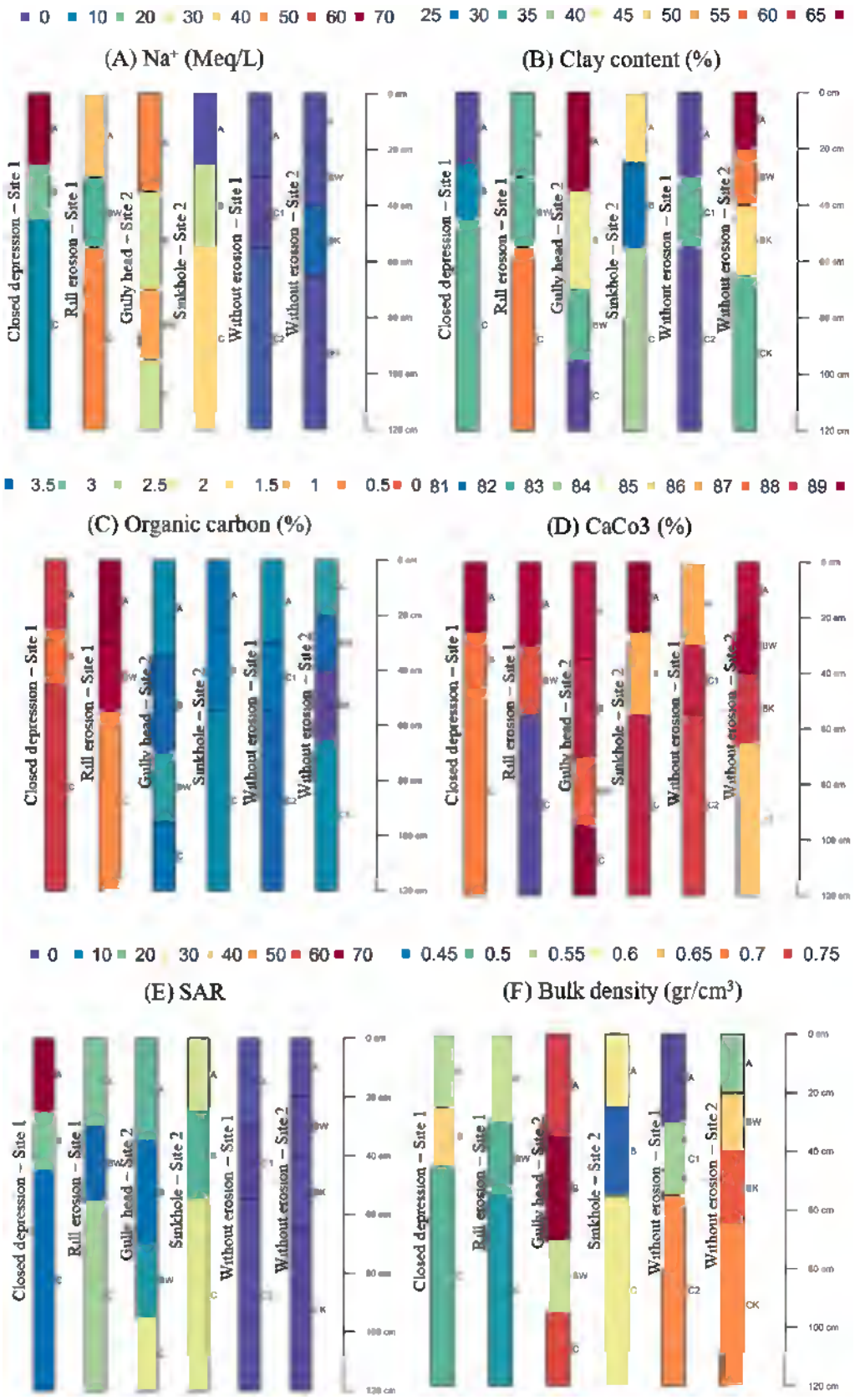

Fig. 8. Soil physical and chemical properties (symbolized with a volume fraction and color) for each soil horizon at Takhte-Soltan (site 1) and Shorluq (site 2).

Table 1
Morphometric features of potential pipes or collapsed cavities corresponding to site 1 (Takhte-Soltan) and site 2 (Shorluq).

	Morphometric features	Average	Min	Max
Site 1 (Takhte-Soltan)	Length (cm)	143.4	40	400
	Depth (cm)	88	30	220
	Volume (m^3)	2.8	0.9	6.9
Site 2 (Shorluq)	Length (cm)	175.7	80	600
	Depth (cm)	79.1	30	170
	Volume (m^3)	2.9	0.3	48.0

pipes were 128.6 m and 227.0 m^3. Accordingly, the ratio of surface erosion features to all (surface erosion features and subsurface potential piping) for length and volume were 0.2 and 0.1, and the length and volume ratio of subsurface potential piping to all were 0.8 and 0.9. Further, the length and volume ratio of surface erosion features to subsurface potential piping were 0.2 and 0.1.

Fig. 10 shows the ERT lines (zoomed to the areas affected by potential pipes and collapsed cavities) investigated at sites 1 and 2. The background resistivity was estimated approximately 10 Ω m due to the almost similar type of materials (marlstone which is including carbonate

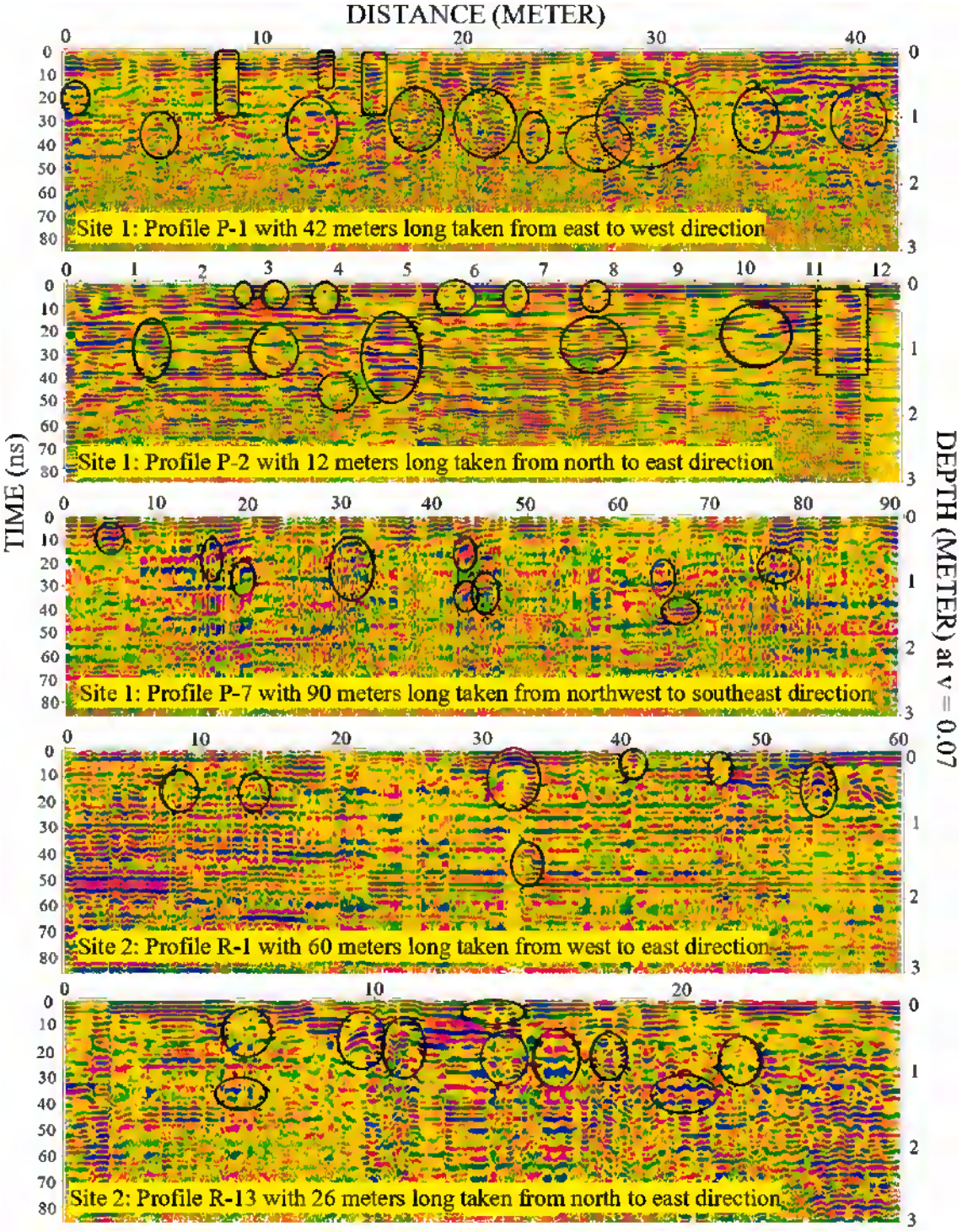

Fig. 9. Examples of GPR lines at site 1 (Takhte-Soltan) and atsite 2 (Shorluq). The circles mark the places with a potential pipe or a collapsed cavity.

Table 2
Characteristics of surface and subsurface (potential) pipes or collapsed cavities corresponding to the Takhte-Soltan site and the Shorluq site.

	Site 1 (Takhte-Soltan)		Site 2)Shorluq(	
	Length	Volume	Length	Volume
Surface erosion features	46.6 *m*	43.6 m^3	24.3 *m*	23.6 m^3
Both surface erosion features and subsurface potential piping	207.9 *m*	293.5 m^3	152.9 *m*	250.6 m^3
Subsurface potential piping	161.3 *m*	249.9 m^3	128.6 *m*	22 m^3
Ratio of surface erosion features to all	0.2	0.1	0.2	0.1
Ratio of subsurface potential piping to all	0.8	0.8	0.8	0.9
Ratio of surface erosion features to subsurface potential piping	0.3	0.2	0.2	0.1

or non-clastic sedimentary rock) at two sites (Reynolds, 2011). Accordingly, the values of electrical resistivity in the sections with potential pipes and collapsed cavities were considered between 30 and 45 Ω m at site 1. However, these values were higher due to the greater size of the potential pipes and collapsed cavities in site 2. In site 1, two ERT profiles were investigated from rangeland with a length of 57 m (Fig. 6A). The ERT-*P*1 was performed in parallel with GPR-P11. The values above 30 Ω m at this point were considered as sites susceptible to potential pipes and collapsed cavities. The position of the anomalies and potential pipes was specified on the cross section (Fig. 10A). At this point, at distances between about 10 m and 12 m, a collapsed pipe was recognized. Afterward, the resistivity values decreased up to distance of 15 m. At distances between 19 m and 25 m, several potential pipes were observed next to each other. At a distance of 26 m, a zone with a smaller resistivity value was also observed. At a distance of 31 m, the resistivity values has decreased to a depth of two meters. At distances between 32 m and 36 m, soil pipes were had collapsed down to a depth of 1 m. At a distance of 40 m, different resistivity values can be seen down to a depth of one meter which corresponds to a layer of shales or mudstones. Also, collapsed pipes were observed at distances ranging from 42 m to 49 m (Fig. 10A). Beside the ERT-*P*1, the ERT-*P*2 was taken in parallel with GPR-P16. The values of electrical resistivity, i.e., more than 30 Ω m at this point, were considered as piping susceptible sites or sites with potential pipes. In this section, two pipe collapses formed at distances between 10 m and 12 m. At distances between 20 m and 25 m, numerous cracks were observed above a layer of basement rocks. The situation was the same at distances between 28 m and 32 m. At distances ranging from 35 m−40 m to 43 m–45 m, diagonal anomalies can be seen reaching the maximum depth of 3 m. The potential pipes and collapsed cavities were also visible at a distance of 47 m (Fig. 10B). In site 2, two ERT profiles ERT-*P*3 and ERT-*P*4 were taken perpendicular to each other, one parallel to profile number GPR-*P*1 and the other in the vertical direction paralleled to GPR-*P*4. These profiles were 57 m long with 110 points in each profile. The ERT-*P*3 was taken in the Shurluq parallel to the GPR-*P*1. The points with values of electrical resistivity larger than 180 Ω m were considered as susceptible sites to potential pipes and collapsed cavities. The location of anomalies or potential pipes was displayed on the cross section (Fig. 10C). In this section, two potential pipes were identified at distances of 7 m and 9 m, and at distances ranging from 18 m to 24 m. At a distance of 33 m, there was a potential pipe or collapsed cavities at a depth of 2 m. These were also observed at distances of 36 m, 40 m, and 43 m. Additionally, The ERT-*P*4 was conducted in parallel with the GPR-*P*4.

The anomaly of each resistivity value was based on its contrast with background resistivity. The only potential pipes in this section had high values of electrical resistivity (>180 Ω m) above the layer of shales or mudstones. At this point, except for a major anomaly that was detected at a distance of about 20 m (surface holes), no other specific anomaly was observed. In general, not only the near surface layers had a significant electrical resistivity, but also the subsurface layers had a detectable electrical resistivity, although the lower layers were more conductive materials with electrical resistivity values between 5 and 30 Ω m. There were a number of rock layers (with electrical resistivity values < 1.90 Ω m) which were wetter than the surrounding layers and these mainly consisted of shales or mudstones.

5. Discussion

In this study, the combination of several methods allowed to better identify subsurface materials and the processes that shaped the land surface. Soil piping is a subsurface process, although it was possible to follow the surface path of soil erosion in the middle and late stages by the determination of drainage density or channel networks using digital elevation models (Fig. 7). This aspect was examined by combining both the surface and subsurface investigations. The UAV images allowed to draw drainage density maps driven from the *ortho*-photo images and to prove that they matched with surface erosional landforms (i.e., dendritic erosion, rill erosion, collapsed pipes). This indicates that pipes were usually present below the surface drainage networks at various depths and with various diameters (Farifteh and Soeters, 1999). In other words, pipes were closely connected to surface rills and sites of preferential flow. Next, they combined into a larhger drainage network. Subsurface drainage in these flow pathways encourages erosional processes, as well as soil collapse events whereby flow pathways amplify their impacts on the drainage network until a collapse element has become visible at the soul surface (Regensburg et al., 2021). The impact of piping erosion on hydrology, channel network, soil erosion, and slope stability was also reported by Bernatek-Jakiel and Poesen (2018).

Besides, visualization of the main soil morphologic properties using “aqp” package helps the interpretation of soil profile information (Beaudette et al., 2013). Different soil properties (clay content, organic carbon, $CaCO_3$, Na^+, Ca^+, and bulk density) which may impact the erodibility were measured in detail for 6 soil profiles with a different position in two studied sites under two land use types, both with and without erosional features. The soils exhibit a large content of silt, which potentially enhances the formation of closed depression in rangelands. However, clay content may increase the number of sinkholes in agricultural land. The investigated soil profiles had a clay loam and clay texture, which may favour piping activity in soils with and without erosional features in the two landuse types. Calcium carbonate content does not differ among the measured soils, although the soil profiles at the sites without erosion are characterized by low Na^+. It should be noted that although the soil attributes favour piping expansion, they themselves do not trigger piping formation (Bernatek-Jakiel et al., 2016). The condition that controls the formation of soil erosional features is the combination of soil properties and hydro-morphological variables (i.e., water infiltration, intense subsurface runoff, steep slopes) in different land uses. Generally, there are small differences in soil attributes at the two landuse types, both with and without soil erosional features. Regardless of the fact that the physical and chemical soil attributes probably initiate erosional processes, soil erosional features were characterized in terms of their location, spatial scale, type along the geomorphological units across agricultural and range land use types. The extent of different erosional features has considerably contributed to the land use types and the hydrogeomorphology.

The assessment of pipe networks was achievable with non-destructive techniques and geophysical tools. Jones and Crane (1984) and Bryan and Jones (1997) underlined that a main problem in the estimation of the piping system was the adversity of finding pipe networks. They highlighted the need for new tools and methods for surveying pipe networks. Wilson et al. (2012) emphasized the use of non-destructive techniques to monitor and evaluate soil pipes and to detect internal erosion. Both ERT and GPR have the potential to study soil pipes, although some restrictions may affect the results. Bernatek-

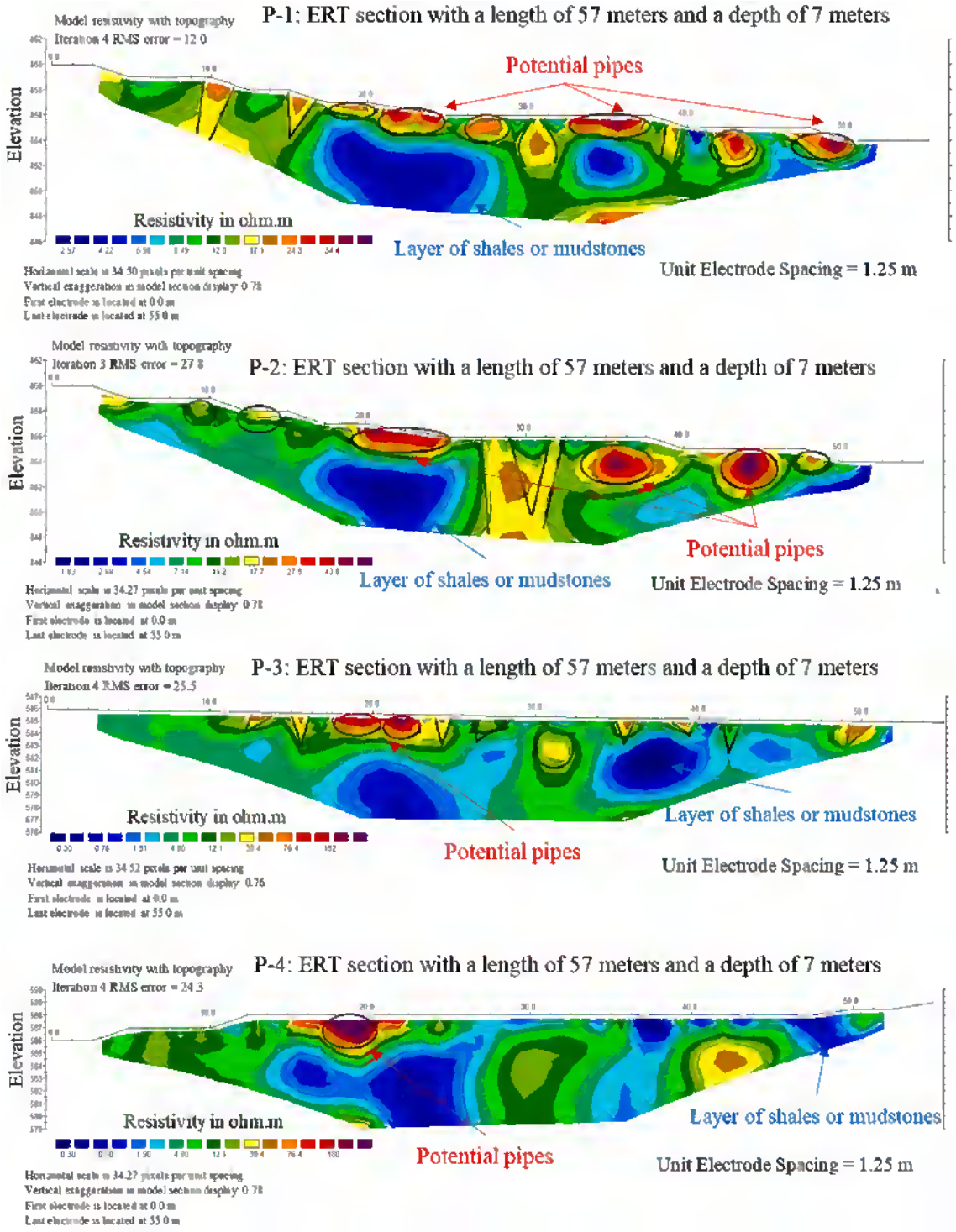

Fig. 10. The depth sections of ERT with an indication of the cross-sectional areas affected by a potential pipe or a collapsed cavity at site 1 (*P*-1 and P-2) and at site 2 (*P*-3 and *P*-4).

Jakiel and Kondracka (2016) applied geophysics tools including GPR and ERT, together with geomorphological mapping for the investigation of piping systems in South Poland. They suggested detailed and basic terrain mapping for the interpretation of ERT and radargrams due to probable disturbances impacting geophysical profiles. The GPR maps produced in this study indicate soil pipes which may transform to consecutive collapses. In some landscapes, this kind of tools displays pipe networks at higher depths (Holden et al., 2002; Bernatek-Jakiel and Kondracka, 2016). Combining all the depths of soil pipes and the visualized soil profiles (Fig. 8) reveals that piping in the study area develops at the boundary of B and C soil horizons. It is in line with Bernatek-Jakiel et al. (2016) who revealed that pipes develop in Cambisols between B and C soil horizons.

Additionally, the volume of surface erosion features and subsurface features at site 1 was 82.9 m^3, whereas the pipe volume below the GPR profiles in the subsurface soil was 317.6 m^3 (Table 2). It showed that the calculation significantly underestimated the area and volume of the piping system by up to 26.1 %. In this case, the total length of the piping

system was underestimated by 28.9 % (ratio of surface length/subsurface length) which confirmed the early stage of piping development as it consists of shallow and few closed depressions, rills, and dendritic erosion channels. At site 2, the soil pipe volume measured according to surface investigations was 23.6 m^3, whereas the pipe volume below the GPR profiles (Table 2) in the subsurface was 227.0 m^3. It showed that measuring soil pipes only at the surface significantly results in an underestimation of the the piping system's volume by up to 10.4 %. The underestimation rate for the total length of pipe systems was 19.9 % in the agricultural lands with large pipes and pipe collapses (single and multiple sinkholes with great length which subsequently become a gully). The estimations made here are very conservative and have many assumptions, and like in other studies this also may underestimate the scale of piping. As reported by Bernatek-Jakiel and Kondracka (2019), the detection of collapsed pipes does not enable the characterization and identification of a complete underground pipe network. It means that soil pipes are not undeviating, they may turn in vertical and horizontal dimensions. It can be concluded that the mean depth of pipe formation was 0.8–0.9 m in rangelands and 0.7–0.8 m in agricultural lands. Also, the total pipe length was 207.9 m out of 600 m (length of the GPR lines) at site 1 and 152.9 m out of 433 m (length of the GPR lines) at site 2. It showed agricultural lands contained pipe collapse features (i.e., sinkholes) that are much larger and more complex than those observed in the rangeland where the number of soil erosion featureswere high, while the soil loss volume is low. It means land use changes are one of the major contributing factors to soil degradation by subsurface erosion in different geomorphological units (Thiam et al., 2021).

The ERT geophysics technique also provides details of the internal soil structure at two different study sites. ERT is not time spending and invasive, and it easily applicable during the field activities and provide the opportunity to assess geotechnical factors of the subsoil and their variation in time and space, constantly screening the subsoil conditions (Sevil et al., 2017; Patti et al., 2021). ERT has been rarely applied in an eroded field, particularly to define the subsurface materials and their associated physical and chemical soil properties or lithology which may have a considerable effect on pipe initiation and expansion. In both examined sites, we analyzed both ERT and soil properties and recognized that the low resistivity values were more related to the layers with high SAR and Na^+ (Fig. 8) at shallow depths in the C horizon, and with shales at larger soil depths. However, the areas affected by piping and their surrounding sites had high resistivity values (Fig. 9), mainly caused by air-filled voids, that decreased at larger depths. This resistivity distribution was associated with the maximum frequency of the pipe depths (Fig. 10). Research on physical and chemical soil properties reports that higher soil porosity, biological activity as well as a silty texture, low bulk density and well-developed soil structure favour subsurface erosional processes (Bernatek-Jakiel et al., 2016; Hosseinalizadeh et al., 2019). In some reports, soil properties together with drainage networks effects were regularly observed as the main drivers of tunnel erosion (Romero Díaz et al., 2007; Verachtert et al., 2013; Kariminejad et al., 2019). The ERT technique also detected voids in regions with more resistivity values. The high resistivity interpreted as the sites with piping occurrences (Oh and Sun, 2008). The lowest resistivity values are found in the impermeable layers of mudstones or shales. The holes or voids observed may be due to the presence of this water restrictive layer, resulting in soil saturation (water accumulation) and piping initiation (see ERT_P4 in Fig. 10). These pipes form because of not only water flow but also because of higher water contents inside pipes (Wilson et al., 2015).

In this study, both GPR and ERT were useful since they showed considerable differences between potential pipes and their surroundings in terms of electrical resistivity and electromagnetic waves (Doolittle and Butnor, 2009). Bernatek-Jakiel and Poesen (2018) underlined the complexity of the mechanisms of piping erosion and the importance of using non-destructive methods in pipe detection in natural landscapes to map the hydrological connectivity of soil pipes. In this study, the GPR and ERT techniques produced high resolution images. Kannaujiya et al. (2019) demonstrated various physical properties of the strata in terms of different dielectric constants in GPR and resistivity in ERT techniques for landslide characterization in India. Bovi et al. (2020) explored the soil properties and geophysics in the context of soil piping. They applied ERT to map the soil pipes and revealed the continuity and connection of the subsurface tunnels. As stated by Bernatek-Jakiel and Kondracka (2022), ERT produces high resolution images of the subsurface representing the alteration in electrical resistivity. However, the combination of geophysical tools in conjunction with field recognition provides an efficient method to identify soil pipes. The integration of these geophysical tools with field observations and UAV remote sensing, is more beneficial to demonstrate the maximum possible piping-prone zone. This study illustrates that earth observation techniques in combination with geophysical tools provides more knowledge about subsurface properties that control piping activity. It was clear that the three-dimensional pipe number density, length, and volume of pipes estimated at the soil surface were much lower than the corresponding values deduced from subsurface observations. This indicates that the role of soil pipes in hillslope hydrology and the formation of gullies can be more important than assumed by observations based on surface techniques (Bernatek-Jakiel and Kondracka, 2016). The GPR and ERT produced valuable results, while other tools including UAV-observations and soil laboratory data analysis provided a better comprehensive understanding of the piping system and its functioning and structure in detecting both surface and subsurface processes. This study contributes to a more comprehensive approach for a better understanding of subsurface pipe networks.

6. Conclusions

The integration of data achieved by geophysical surveys and UAV remote sensing provides quantitative and valuable data for the investigation of piping distribution in two study areas. The channel networks, observed by UAV and their relation to mapped pipes and gullies showed how well the surface drainage lines relate to these erosion features. The physical and chemical soil attributes may also control soil pipe formation, but they themselves are not enough to explain piping development at the two study sites. The investigations at the two study sites shows the suitability of ERT and GPR applications to measure pipe networks. Generally, geophysical tools allow to collect information on the presence of potential soil pipes, pipe volume and density, and the identification of the internal structure and materials where soil pipes occur. The benefit of GPR is that it permits the recognition of the spatial distribution of soil pipes, thus, leading to a better assessment of the soil piping scale. Potential pipes and collapsed cavities in rangelands (site 1) develop at a mean soil depth of about 0.8–0.9 m with a pipe number density of 5.1 m^{-3}. The mean soil depth for potential pipes and collapsed cavities in agricultural lands is about 0.7–0.8 m with a pipe number density of 1.8 m^{-3}. According to the geophysical survey at site 1, the total erosion features volume at the surface is 82.9 m^3, whereas it is 317.6 m^3 in the subsurface. According to geophysical survey at site 2, the volume of erosion features at the surface is 23.6 m^3 and 226.9 m^3 in the subsurface. This means that the subsurface volume of soil pipes at the two study sites appears to be remarkably higher than that only mapped on the basis of surface observations. This points to a significant underestimation of soil piping in both rangelands and agricultural lands, where these soil processes have been largely neglected in the last decades.

The experimental work with ERT for characterizing soil piping indicates the subsoil boundary of soil pipe evolution and the soil attributes that affect piping in the Sarakhs plain, Razavi Khorasan Province. The ERT profiles showed soil zones impacted by soil pipes as places of greater resistivity values, which result from a greater volume of air-filled pores (due to intense biological activity, greater soil porosity, and well-developed soil structure). Additionally, the ERT profiles reveal that pipes in agricultural lands and rangelands develop at the soil bedrock interface, sometimes above layers of mudstones or shales, that create a

water restrictive layer. While ERT and GPR data may be interpreted more accurately, they nonetheless allow one to better understand soil piping. By integrating these data with UAV mapping and visualization of soil attributes, they provide a basis for the statistical analysis for a more accurate estimation of soil pipe volumes. The identification of soil piping processes is essential to know its role in hillslope hydrology and the formation of gullies, not only in pediments under a semi-arid climate, but also globally.

Declaration of Competing Interest

The authors declare that they have no known competing financial interests or personal relationships that could have appeared to influence the work reported in this paper.

Data availability

The authors do not have permission to share data.

Acknowledgments

This research is supported by the Ferdowsi University of Mashhad (FUM), Mashhad, Iran, as part of a post-doctoral research project. The authors are grateful to the Deputy of Research and Technology of the FUM for financial support of the project (grant No. 20.1.1400).

References

Beaudette, D.E., Roudier, P., O'Geen, A.T., 2013. Algorithms for quantitative pedology: A toolkit for soil scientists. Comput. Geosci. 52, 258–268.
Bernatek-Jakiel, A., Kacprzak, A., Stolarczyk, M., 2016. Impact of soil characteristics on piping activity in a mountainous area under a temperate climate (Bieszczady Mts., Eastern Carpathians). Catena 141, 117–129.
Bernatek-Jakiel, A., Kondracka, M., 2016. Combining geomorphological mapping and near surface geophysics (GPR and ERT) to study piping systems. Geomorphology 274, 193–209.
Bernatek-Jakiel, A., Kondracka, M., 2019. Detection of soil pipes using ground penetrating radar. Rem. Sen. 11 (16), 1864.
Bernatek-Jakiel, A., Kondracka, M., 2022. Detection of soil pipe network by geophysical approach: Electromagnetic induction (EMI) and electrical resistivity tomography (ERT). Land Degrad. Dev. 33 (7), 1002–1014.
Bernatek-Jakiel, A., Poesen, J., 2018. Subsurface erosion by soil piping: significance and research needs. Earth-Sci. Rev. 185, 1107–1128.
Bíl, M., Kubeček, J., 2012. Piping in loess-like and loess-derived soils: Case study of Halenkovice site, Czech Republic. Ann. Soc. Geol. Pol. 82, 45–50.
Blake, G.R., Hartge, K.H., 1986. Bulk density. Methods of Soil Analysis: Part 1 Physical and Mineralogical Methods 5:, 363–375.
Botschek, J., Krause, S., Abel, T., Skowronek, A., 2002. Piping and erodibility of loessic soils in Bergisches Land, Nordrhein-Westfalen. J. Plant Nutr. Soil Sci. 165 (2), 241–246.
Boucher, S.C., 1990. Field Tunnel Erosion, its Characteristics and Amelioration. Dept. of Conservation and Environment, Land Protection Division.
Bovi, R.C., Moreira, C.A., Rosolen, V.S., Rosa, F.T.G., Furlan, L.M., Helene, L.P.I., 2020. Piping process: Genesis and network characterization through a pedological and geophysical approach. Geoderma 361, 114101.
Bryan, R.B., Jones, J.A.A., 1997. The significance of soil piping processes: Inventory and prospect. Geomorphology (Amsterdam) 20 (3–4), 209–218.
Cappadonia, C., Coco, L., Buccolini, M., Rotigliano, E., 2015. From slope morphometry to morphogenetic processes: An integrated approach of field survey, geographic information system morphometric analysis and statistics in Italian badlands. Land Degrad. Dev. 27 (3), 851–862.
Carbonel, D., Rodríguez, V., Gutiérrez, F., McCalpin, J.P., Linares, R., Roqué, C., Zarroca, M., Guerrero, J., Sasowsky, I., 2014. Evaluation of trenching, ground penetrating radar (GPR) and electrical resistivity tomography (ERT) for sinkhole characterization. Earth Surf. Proc. Land. 39 (2), 214–227.
Chappell, N.A., Sherlock, M.D., 2005. Contrasting flow pathways within tropical forest slopes of Ultisol soils. Earth Surf. Proc. Land. 30 (6), 735–753.
Color, M., (Firm)., 2010. Munsell Soil Color Charts: With Genuine Munsell Color Chips. Munsell Color, Grand Rapids, MI.
Doolittle, J.A., Butnor, J.R., 2009. Soils, peatlands and biomonitoring. In: Jol, H.M. (Ed.), Ground Penetrating Radar: Theory and Applications. Elsevier Science, pp. 179–202.
Evangelista, L., de Silva, F., d'Onofrio, A., Di Fiore, V., Silvestri, F., di Santolo, A.S., Cavuoto, G., Punzo, M., Tarallo, D., 2017. Application of ERT and GPR geophysical testing to the subsoil characterization of cultural heritage sites in Napoli (Italy). Measurement 104, 326–335.
Farifteh, J., Soeters, R., 1999. Factors underlying piping in the Basilicata region, southern Italy. Geomorphology 26 (4), 239–251.
Faulkner, H., 2006. Piping hazard on collapsible and dispersive soils in Europe. Soil Eros. Europe 22, 537–562.
Galarowski, T., 1976. New observations of the present-day suffosion (piping) processes in the Bereźnica catchment basin in The Bieszczady Mountains (The East Carpathians). Studia Geomorphologica Carpatho-Balcanica 10, 115–124.
Gee GW, Bauder JW. 1986. Particle-size analysis. In: Klute, A. Ed, Methods of Soil Analysis: Part 1. Ž. Physical and Mineralogical Methods, 2nd edn, Agronomy, 9. Soil Science Society of America, Madison, USA, pp. 383–411.
J.B. Got P. André L. Mertens C. Bielders S. Lambot Soil piping: networks characterization using ground-penetrating radar 2014 Brussels, Belgium 144 148.
Hamshaw, S.D., Engel, T., Rizzo, D.M., O'Neil-Dunne, J., Dewoolkar, M.M., 2019. Application of unmanned aircraft system (UAS) for monitoring bank erosion along river corridors. Geomat. Nat. Hazards Risk 10 (1), 1285–1305.
Holden, J., Burt, T.P., Vilas, M., 2002. Application of ground-penetrating radar to the identification of subsurface piping in blanket peat. Earth Surf. Proc. Land. 27 (3), 235–249.
Hosseinalizadeh, M., Kariminejad, N., Chen, W., Pourghasemi, H.R., Alinejad, M., Behbahani, A.M., Tiefenbacher, J.P., 2019. Gully headcut susceptibility modeling using functional trees, naïve Bayes tree, and random forest models. Geoderma 342, 1–11.
Johansson, S., Dahlin, T., 1996. Seepage monitoring in an earth embankment dam by repeated resistivity measurements. Eur. J. Eng. Environ. Geophys. 1 (3), 229–247.
Jol, H.M., 2008. Ground Penetrating Radar Theory and Applications. Elsevier.
Jones, J.A.A., 2004. Implications of natural soil piping for basin management in upland Britain. Land Degrad. Dev. 15 (3), 325–349.
Jones, J.A.A., 2010. Soil piping and catchment response. Hydrol. Process. 24 (12), 1548–1566.
Jones, J.A., Crane, F.G., 1984. Pipe flow and pipe erosion in the Maesnant experimental catchment. In: In *International Geographical Union Commission on field experiments In geomorphology. MeetIng*, pp. 55–72.
Kannaujiya, S., Chattoraj, S.L., Jayalath, D., Bajaj, K., Podali, S., Bisht, M.P.S., 2019. Integration of satellite remote sensing and geophysical techniques (electrical resistivity tomography and ground penetrating radar) for landslide characterization at Kunjethi (Kalimath), Garhwal Himalaya, India. Nat. Hazards 97 (3), 1191–1208.
Kariminejad, N., Hosseinalizadeh, M., Pourghasemi, H.R., Bernatek-Jakiel, A., Alinejad, M., 2019. GIS-based susceptibility assessment of the occurrence of gully headcuts and pipe collapses in a semi-arid environment: Golestan Province, NE Iran. Land Degradat. Develop. 30 (18), 2211–2225.
Kariminejad, N., Hosseinalizadeh, M., Pourghasemi, H.R., Tiefenbacher, J.P., 2021. Change detection in piping, gully head forms, and mechanisms. Catena 206, 105550.
Kasprzak, M., Strzelecki, M.C., Traczyk, A., Kondracka, M., Lim, M., Migała, K., 2017. On the potential for a bottom active layer below coastal permafrost: The impact of seawater on permafrost degradation imaged by electrical resistivity tomography (Hornsund, SW Spitsbergen). Geomorphology 293, 347–359.
Loeppert, R.H., Suarez, D.L., 1996. Carbonate and gypsum. Methods Soil Analysis 3, 437–474.
Mayr, A., Bremer, M., Rutzinger, M., Geitner, C., 2019. Unmanned aerial vehicle laser scanning for erosion monitoring in alpine grassland. ISPRS Ann. Photogram. Rem. Sens. Spat. Inform. Sci. 29, 4.
Migoń, P., Kacprzak, A., Malik, I., Kasprzak, M., Owczarek, P., Wistuba, M., Pánek, T., 2014. Geomorphological, pedological and dendrochronological signatures of a relict landslide terrain, Mt Garbatka (Kamienne Mts), SW Poland. Geomorphology 219, 213–231.
Nelson DW, Sommers L. 1983. Total carbon, organic carbon, and organic matter. *Methods of soil analysis: Part 2 chemical and microbiological properties* **9**: 539-579.
Oh, S., 2012. Safety assessment of dams by analysis of the electrical properties of the embankment material. Eng. Geol. 129, 76–90.
Oh, S., Sun, C., 2008. Combined analysis of electrical resistivity and geotechnical SPT blow counts for the safety assessment of fill dam. Environ. Geol. 54 (1), 31–42.
Panthulu, T.V., Krishnaiah, C., Shirke, J.M., 2001. Detection of seepage paths in earth dams using self-potential and electrical resistivity methods. Eng. Geol. 59 (3–4), 281–295.
Patti, G., Grassi, S., Morreale, G., Corrao, M., Imposa, S., 2021. Geophysical surveys integrated with rainfall data analysis for the study of soil piping phenomena occurred in a densely urbanized area in eastern Sicily. Nat. Hazards 108 (3), 2467–2492.
Podgorski, J.E., Green, A.G., Kalscheuer, T., Kinzelbach, W.K., Horstmeyer, H., Maurer, H., Rabenstein, L., Doetsch, J., Auken, E., Ngwisanyi, T., Tshoso, G., 2015. Integrated interpretation of helicopter and ground-based geophysical data recorded within the Okavango Delta, Botswana. J. Appl. Geophys. 114, 52–67.
Poesen, J., 2018. Soil erosion in the Anthropocene: Research needs. Earth Surf. Proc. Land. 43 (1), 64–84.
Poesen, J., Vandaele, K., van Wesemael, B., 1996. Contribution of Gully Erosion to Sediment Production in Cultivated Lands and Rangelands, IAHS Publication 236. IAHS Press, Wallingford, pp. 251–266.
Reynolds, J.M., 2011. An introduction to Applied and Environmental Geophysics. John Wiley & Sons.
Robinson M, Bristow C, McKinley J, Ruffell A. 2013, 1(5), pp. 5. Ground Penetrating Radar. Geomorphological Techniques (Online Edition). British Society for Geomorphology, London. ISSN, pp. 2047–0371.
Regensburg TH, Chapman PJ, Pilkington MG, Chandler DM, Evans MG, Holden J Effects of pipe outlet blocking on hydrological functioning in a degraded blanket peatland Hydrological Processes 35 3 2021 e14102.
Romero Díaz, A., Marín Sanleandro, P., Sánchez Soriano, A., Belmonte Serrato, F., Faulkner, H., 2007. The causes of piping in a set of abandoned agricultural terraces in southeast Spain. Catena 69, 282–293.

Schrott, L., Sass, O., 2008. Application of field geophysics in geomorphology: Advances and limitations exemplified by case studies. Geomorphology 93 (1–2), 55–73.
Sevil, J., Gutiérrez, F., Zarroca, M., Desir, G., Carbonel, D., Guerrero, J., Linares, R., Roqué, C., Fabregat, I., 2017. Sinkhole investigation in an urban area by trenching in combination with GPR, ERT and high-precision leveling. Mantled evaporite karst of Zaragoza city, NE Spain. Eng. Geol. 231, 9–20.
Sjödahl, P., Dahlin, T., Johansson, S., 2009. Embankment dam seepage evaluation from resistivity monitoring data. Near Surf. Geophys. 7 (5–6), 463–474.
Smart, R.P., Holden, J., Dinsmore, K.J., Baird, A.J., Billett, M.F., Chapman, P.J., Grayson, R., 2013. The dynamics of natural pipe hydrological behavior in blanket peat. Hydrol. Process. 27 (11), 1523–1534.
Starkel, L., 2006. Geomorphic hazards in the Polish flysch Carpathians. Studia Geomorphologica Carpatho-Balcanica 40, 7–19.
Tandon, R.S., Gupta, V., Venkateshwarlu, B., 2021. Geological, geotechnical, and GPR investigations along the Mansa Devi hill-bypass (MDHB) Road, Uttarakhand, India. Landslides 18 (3), 849–863.
Thiam, S., Villamor, G.B., Faye, L.C., Sène, J.H.B., Diwediga, B., Kyei-Baffour, N., 2021. Monitoring land use and soil salinity changes in coastal landscape: A case study from Senegal. Environ. Monit. Assess. 193 (5), 1–18.
Vasu, D., Singh, S.K., Ray, S.K., Duraisami, V.P., Tiwary, P., Chandran, P., Nimkar, A.M., Anantwar, S.G., 2016. Soil quality index (SQI) as a tool to evaluate crop productivity in semi-arid Deccan plateau, India. Geoderma 282, 70–79.
Van Schoor, M., 2002. Detection of sinkholes using 2D electrical resistivity imaging. J. Appl. Geophys. 50 (4), 393–399.
Verachtert, E., Van Den Eeckhaut, M., Poesen, J., Deckers, J., 2010. Factors controlling the spatial distribution of soil piping erosion on loess-derived soils: A case study from central Belgium. Geomorphology 118 (3–4), 339–348.
Verachtert, E., Maetens, W., Van Den Eeckhaut, M., Poesen, J., Deckers, J., 2011. Soil loss rates due to piping erosion. Earth Surf. Proc. Land. 36 (13), 1715–1725.
Verachtert, E., Van Den Eeckhaut, M., Martínez-Murillo, J.F., Nadal-Romero, E., Poesen, J., Devoldere, S., Wijnants, N., Deckers, J., 2013. Impact of soil characteristics and land use on pipe erosion in a temperate humid climate: Field studies in Belgium. Geomorphology 192, 1–14.
Wilson, G.V., Nieber, J.L., Sidle, R.C., Fox, G.A., 2012. Internal erosion during soil pipe flow: State of the science for experimental and numerical analysis. Trans. ASABE 56 (2), 465–478.
Wilson, G.V., Rigby, J.R., Dabney, S.M., 2015. Soil pipe collapses in a loess pasture of Goodwin Creek watershed, Mississippi: role of soil properties and past land use. Earth Surf. Proc. Land. 40 (11), 1448–1463.
Wilson, G.V., Wells, R., Kuhnle, R., Fox, G., Nieber, J., 2018. Sediment detachment and transport processes associated with internal erosion of soil pipes. Earth Surf. Proc. Land. 43 (1), 45–63.
Zhu, T.X., 2012. Gully and tunnel erosion in the hilly Loess Plateau region, China. Geomorphology 153, 144–155.